Editors' Suggestion

# Anticorrelation between excitations and locally favored structures in glass-forming systems

Danqi Lang [1,2,*] Camille Scalliet [3] and C. Patrick Royall [1]

[1] *Gulliver UMR CNRS 7083, ESPCI Paris, Université PSL, 75005 Paris, France*

[2] *Département de Physique de l'Ecole Normale Supérieure, ENS, Université PSL, 75005 Paris, France*

[3] *Laboratoire de Physique de l'Ecole normale supérieure, ENS, Université PSL, CNRS, Sorbonne Université, Université Paris Cité, 75005 Paris, France*

(Received 13 September 2024; accepted 19 March 2025; published 23 May 2025)

Dynamics that are microscopic in space and time, where particles commit to a new position, referred to as excitations, are considered the elementary unit of relaxation in the dynamic facilitation theory of the glass transition. Meanwhile, geometric motifs known as locally favored structures are associated with vitrification in many glassformers. Recent work indicates that the probability of particles being found in both locally favored structures (LFS) and excitations decreases significantly upon supercooling, suggesting an anticorrelation between them [Ortlieb *et al.*, Nat. Commun. **14**, 2621 (2023)]. However, the spatial relationship between excitations and LFS remains unclear. By employing state-of-the-art GPU computer simulations and colloid experiments, we analyze this relationship in model glassformers. We reveal a strong anti-correlation between long-lived LFS and excitations, along with a spatial separation between the two in deeply supercooled liquids. This strong anticorrelation likely arises because well-packed LFS resist local rearrangements, and thus hindering the formation of excitations.

DOI: 10.1103/PhysRevE.111.055415

## I. INTRODUCTION

The process of vitrification, whereby a liquid solidifies without crystallizing, remains a major challenge in condensed matter. There are a variety of theories postulated, which provide equally good descriptions of the observed dynamic slowdown of some fourteen orders of magnitude in relaxation time with respect to the high-temperature liquid [1]. Some are even considered incompatible. For instance, certain theories relate the dynamic slowdown to a thermodynamic transition into a putative amorphous state with subextensive configurational entropy, known as the ideal glass [2,3]. Others, however, propose that the glass transition is primarily a dynamical phenomenon, where thermodynamics is not important and no reference is made to the structure of the material [4,5]. Still other theories connect the glass transition to the emergence of geometric motifs associated with local order, referred to as locally favored structures (LFS). These structures may be amorphous [6,7] or crystalline [8].

Particle-resolved studies, using computer simulation or optical imaging of colloids [9–12] promise the level of detail to discriminate between the predictions made by these competing theoretical descriptions. However, until recently, such studies were confined to the weakly supercooled regime well described by the mode-coupling theory (MCT) [13], corresponding to approximately four orders of magnitude increase in relaxation time. Particle-resolved data obtained at deeper supercooling, below the MCT crossover, is needed to make progress. Recently, such data has become available, using particle-swap Monte Carlo algorithms [14–16], and efficient GPU-based molecular dynamics [17]. Colloid experiments too have passed the MCT crossover by using smaller particles [18–20]. However, rather than providing clear support for one particular theoretical approach, these new data seem to support multiple theories. One of these is dynamic facilitation theory (DF) [4,5,21] which predicts that relaxation occurs by dynamic excitations which are microscopic in space and time. Excitations are indeed found at the relevant population, size, and duration in simulations [20–23] and experiments [12,24]. On the other hand the cooperatively rearranging regions (CRRs) envisioned by the thermodynamics-based approaches of the random first-order transition theory (RFOT) [3] and Adam-Gibbs theory [2] are expected to grow in size and massively in timescale upon supercooling. These too are found, consistent with theory, in particular the prediction of their compaction at deep supercooling is upheld [20,25]. In addition, a drop in configurational entropy upon supercooling has been observed in a number of studies [19,26–28]. It has been suggested that these two approaches may be reconciled [16,20,29,30], potentially offering a unified perspective on the glass transition problem.

Central to addressing the challenge of identifying which theory of the glass transition is most effective is understanding the relationship between microscopic structure and dynamics in glassforming systems. A probe of this relationship is the isoconfigurational ensemble, which is a computational technique. Here an ensemble of trajectories is run from the same initial coordinates [31]. Its predictability of the dynamics at short lengthscales has been questioned [32], but information theoretic methods have shown some correlation with LFS [33,34], and that this is highly dependent on the system chosen [35]. More recently, machine-learning methods have found a more significant predictability based on the cage of neighbors

*Contact author: danqilang@gmail.com

 

of a given particle [36]. This suggests a clear relationship between structure and dynamics in glassforming systems, contrary to the principles of DF which was conceived in the context of kinetically constrained models. The latter may be ideal gases from a thermodynamic perspective and explicitly lack structural correlations [4,5].

A further link between DF and local structure was established by the observation that the time-averaged population of LFS can drive a dynamical phase transition which is a central ingredient of DF [4,26,37]. This suggests that there is at least some structural component to dynamic facilitation, at least in atomistic models. A very recent unexpected finding is an anticorrelation between LFS and particles in excitations [20]. Furthermore, the anticorrelation between excitations and LFS was found to be stronger than that between CRRs and LFS. This is surprising given that the CRRs are expected to be regions of higher configurational entropy and LFS have been shown to be correlated with low configurational entropy [19,38].

The fact that it is now possible to study glass formers at the single-particle level in real space at deeper supercooling than the mode-coupling crossover opens the way to probe the role of LFS in this newly accessible dynamical regime. The unexpected anticorrelation between LFS and excitations [20] motivates further investigation into their relationship, particularly under conditions of deeper supercooling. If LFS are imagined to be more stable than other regions of the system, one might expect them to "expel" excitations upon supercooling. To test this hypothesis, we employ GPU-based simulations of a model glassformer and conduct colloidal experiments.

This paper is organized as follows. In Sec. II we describe our computational and experimental models and methods. We present our results in Sec. III. Our findings are discussed in Sec. IV and we conclude in Sec. V. Additional results may be found in the Appendix.

## II. METHODS

### A. Details of computer simulations

We study the Kob-Andersen (KA) binary Lennard-Jones (LJ) mixture at 2:1 and 3:1 compositions with particle density $\rho = 1.4$. The system size is $N = 10\,002$ for the 2:1 composition and $N = 10\,000$ for 3:1. We also simulate the 4:1 composition at particle density $\rho = 1.204$ with a system size of $N = 10\,000$. This composition is prone to crystallize below the mode-coupling crossover [39]. In the KA mixture, the interaction potential between two particles $i$ and $j$ separated by a distance $r_{ij}$ is

$$u(r_{ij}) = 4\epsilon_{\alpha\beta}\left[\left(\frac{\sigma_{\alpha\beta}}{r_{ij}}\right)^{12} - \left(\frac{\sigma_{\alpha\beta}}{r_{ij}}\right)^{6}\right], \tag{1}$$

where $\alpha, \beta = A, B$ are the two particle types, with parameters $\sigma_{AA} = 1$, $\sigma_{AB} = 0.80$, $\sigma_{BB} = 0.88$, and $\epsilon_{AA} = 1$, $\epsilon_{AB} = 1.50$, $\epsilon_{BB} = 0.50$. The potential is cut off for $r_{ij} > 2.5\sigma_{AB}$. We employ $m_A = m_B = 1$. Times are expressed in units of $\sigma_{AA}\sqrt{m_A/\epsilon_{AA}}$.

Computer simulations were carried out using Roskilde University Molecular Dynamics (RUMD) package [17]. RUMD addresses the challenge of utilizing the many-core nature of modern GPU hardware when simulating small to medium system sizes, as investigated here. Such an implementation makes it possible to probe the system at low temperatures in equilibrium conditions, where the structural relaxation time $\tau_\alpha$ may be larger than $10^6$. More details on the RUMD implementation can be found in the original reference [17].

We simulate the systems in equilibrated conditions at temperature $T = 0.48, 0.49, 0.50, 0.52, 0.55$ for the 2:1 composition, and $T = 0.68, 0.7, 0.73, 0.75, 0.8$ for the 3:1 case. Once thermalization is reached at these temperatures, we use the LAMMPS package [40,41] to produce short trajectories of 1000 LJ time units. The simulations are run in the NVT ensemble, with a timestep $dt = 0.005$. We sample configurations at a time interval of 1 LJ time unit along the trajectory in order to identify excitations and LFS. For each temperature, we produce ten independent trajectories. The results presented below correspond to an average over these independent runs.

We employ the conjugate gradient method to find the inherent structure (IS) of each sampled configuration. Both LFS and excitation analyses are conducted using the IS trajectories, as these provide a stronger anticorrelation compared to thermalized trajectories.

### B. Experimental details

We carry out confocal microscopy experiments with colloidal particles which we track at the single particle level in space and time. These particles closely approximate the hard sphere model [11,42]. We use fluorescently labeled density and refractive index matched colloids of sterically stabilized polymethyl methacrylate. The diameter of the colloids is $\sigma^{\text{exp}} = 3.23$ μm and the polydispersity is 6% which is sufficient to suppress crystallization. The Brownian time to diffuse a radius is $\tau_B = 6.06$ s. The particles were labeled with the fluorescent dye 3,3′-dioctadecyloxacarbocyanine perchlorate ($\text{DiOC}_{18}$). Further details are available in Royall *et al.* [42].

The glass transition of hard spheres is obtained via compression, or increasing the volume fraction $\phi$. A convenient quantity to express the state point is the reduced (osmotic) pressure $Z = \beta P/\rho$ [43], with $\beta = 1/k_B T$ the inverse thermal energy, $P$ the pressure, and $\rho$ the number density. Here $Z$ is determined from the Carnahan-Starling relation

$$Z = \frac{1 + \phi + \phi^2 - \phi^3}{(1-\phi)^3}. \tag{2}$$

Although the colloidal system approaches its glass transition via compression rather than cooling, to facilitate comparison with the simulations and, more generally, molecular systems, we still refer to the colloidal system as being supercooled [11].

We consider two state points, $\phi = 0.587$ and $\phi = 0.593$, corresponding to $Z = 24.54$ and $Z = 25.75$. The trajectories last $421\tau_B$ and $4270\tau_B$, containing 256 and 431 configurations, respectively.

### C. Detecting excitations

We first describe the procedure to detect excitations in simulations and experiments, based on the algorithm proposed by Ortlieb *et al.* [20]. We analyze molecular dynamics data

applying this algorithm to the inherent state trajectory, instead of the thermal one. In short, the method analyzes the coordinates of each particle and searches for sudden motion, corresponding to dynamic excitations. More specifically, the algorithm to detect excitations in simulations follows these steps:

(i) *Check for particle motion.* We compare the position of the particle at the beginning and the end of the trajectory. We compute its average position over the first and last intervals of duration $t_a = 200$ LJ time units. If the particle displacement is less than a threshold $a$, the particle is not considered an excitation. We choose $a = 0.5\sigma$ to ensure that the identified excitations are likely contributing to the $\alpha-$relaxation, and remark that our method does not exclude excitations with $\Delta x > 0.5\sigma$.

(ii) *Identify the excitation time.* We analyze particle trajectories by fitting their position time series with a hyperbolic tangent function. This fit is applied within a sliding time window of width $2t_a$, where each frame is initially considered as the center of the window (potentially indicating a jump in particle position, and thus the location of an excitation). The excitation time, $t_0$, is identified as the center of the time window where the fit is locally optimal. Occasionally (<5% of cases), a single particle trajectory may exhibit multiple excitations. If two locally optimal fits result in excitation times $t_0$ that are separated by more than $t_a$, we treat them as distinct excitations. From the fitting process, we also extract the duration of each excitation, $\Delta t$, and the corresponding displacement, $\Delta x$.

(iii) *Exclude slow and small motion.* We exclude particles from being classified as excitations if they correspond to slow $\Delta t > 0.75t_a$ or small $\Delta x < a$ motion.

(iv) *Ensure the commitment of the particle to its new position.* We extend the MD trajectories by an additional 1000 LJ time units. We compare their average positions during the first and last $t_a$ within the total 2000 LJ time units. Particles with displacements smaller than $a$ are excluded from the analysis.

(v) Particles that satisfy all the above criteria are considered to be in excitations.

To analyze experimental trajectories, we employ a similar protocol and make the following adjustments. First, we define excitations considering the thermalized trajectories, given that inherent structures are not defined for experiments on hard colloids. In step (i), we consider windows of duration $t_a = 200\tau_B$. The threshold distance to define excitations in steps (i) and (iii) is also taken to be $a = 0.5\sigma^{\text{exp}}$. Finally, given the short duration of the experiment, especially at $\phi = 0.587$, we skip step (iv) and do not check that the colloids commit to their new position over longer experimental timescales.

Once individual excitations are identified, we compute their concentration $c_a$, defined as the number of excitations found per trajectory (containing 1000 configurations for simulations). For the experiments, we analyzed 256 and 431 frames for effective volume fractions $\phi = 0.587$ and $\phi = 0.593$, respectively.

### D. Identifying long-lived LFS

We now turn to the identification of LFS. To probe LFS in the Kob-Andersen mixtures and hard sphere colloids, we use the topological cluster classification (TCC) algorithm [44]. As for excitations, we consider configurations in their inherent structure for simulations and thermalized ones for experiments. By comparing the lifetime of various LFS, previous studies have identified the dominant structures as the bicapped square antiprism for the KA model (for all compositions studied here) and the defective icosahedron for hard sphere colloids [34,45–48]. These LFS are depicted in Fig. 1(b) and are comprised of 11 and 10 particles, respectively. The bicapped square antiprism has a maximal number of energetically favorable A-B bonds for the central B particle, which may contribute to its comparatively longer lifetime among the identified structures [46].

The initial step of the TCC algorithm involves identifying bonds between neighboring particles. These bonds are detected using a modified Voronoi method, with a maximum bond length $r_c = 2.0$ for all pairs. For the KA model, we take the parameter $f_c = 1$ to control the identification of four-membered rings as opposed to three-membered rings. In the case of the experiments $f_c = 0.82$ for hard spheres, and all particles are treated equally (we neglect polydispersity following previous works [34,46,48]).

After identifying the LFS in each configuration, we define their lifetime and select those that are long lived. It was shown that particles can leave a LFS for a short time (less than around $0.1\tau_\alpha$) and return to it [46,48,49]. Since the $\alpha$-relaxation time is longer than the trajectory, we allow particles to leave the LFS provided it reforms during the trajectory. We therefore define the lifetime of the $i$th instance of a LFS as the duration for which the instance is continuously detected between two configurations in a trajectory

$$\tau_{\text{lfs},i} = t_i^{\text{end}} - t_i^{\text{init}}, \tag{3}$$

where $t_i^{\text{init}}$ and $t_i^{\text{end}}$ represent the initial and final times, respectively. The same LFS may occur in more than one instance and have an associated lifetime for each $\tau_{\text{lfs},1}$, $\tau_{\text{lfs},2}$, ...,. Thus we define the lifetime of a LFS as the summation of all instances

$$\tau_{\text{lfs}} = \sum_i \tau_{\text{lfs},i}. \tag{4}$$

It has previously been shown that around the mode-coupling crossover, LFS have a lifetime around $\tau_\alpha$ under a criterion that 10% of the original population remain [48]. We find that this holds at the lower temperatures, implying that typical LFS lifetimes very much exceed the trajectory lengths that are practical to identify excitations. Indeed, the cumulative probability distributions of LFS lifetimes $\tau_{\text{lfs}}$ shown in Fig. 8 of the Appendix are limited due to the finite trajectory length. We therefore make an arbitrary selection for a LFS to be considered "long lived" as those persisting for more than 800 LJ time units in simulation. We have confirmed that extending the trajectory (to 2000 and 3000 LJ time units) has only a small effect on the number of LFS identified as long lived and no effect on our conclusions. In the case of the experiments, the trajectory length is closer to the structural relaxation time. Here we set the threshold for long-lived LFS to $170\tau_B$ (resp. $1700\tau_B$) for the experiment at $\phi = 0.587$ (resp. $\phi = 0.593$). In the following, our analysis is based on long-lived LFS.

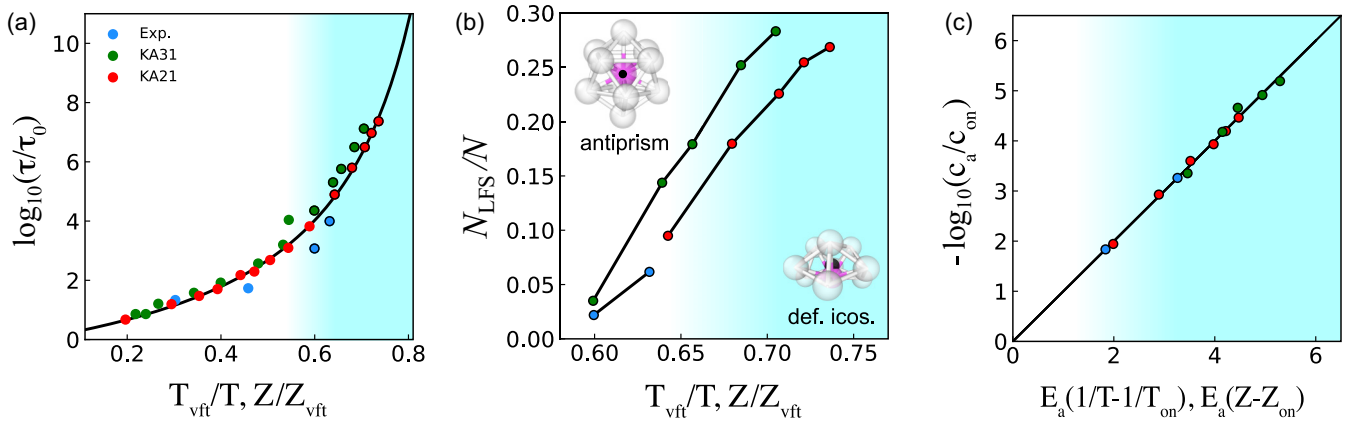


FIG. 1. Characteristics of the systems considered. (a) Relaxation time $\tau_\alpha$ with inverse temperature $T$ for Kob-Andersen binary (KA) mixtures (data from Ortlieb *et al.* [20]) and compressibility $Z$ for the hard-sphere colloidal system (data from Royall *et al.* [42]), scaled with Vogel-Fulcher-Tamman (VFT) parameters given in Table I. The black line is the VFT fit for KA 2:1. We perform our analysis for the data points circled in black, below the mode-coupling crossover (blue shading). (b) Population of long-lived LFS: the bicapped square antiprism for KA mixtures (top left), and the defective icosahedron for the experimental colloidal system (bottom right). The pink particle is considered the central particle, while the black point is the geometric center of the LFS. (c) Scaling of the excitation concentration $c_a$, with the fitting parameters given in Table II.

### E. Measuring the separation between excitations and LFS

If a particle is found to belong to a long-lived LFS, we label it as "LFS" throughout the trajectory. For excitations, we label the particle as "EX" during $[t_0 - t_a, t_0 + t_a]$, where $t_0$ is the time at which the excitation occurs. We use different time criteria for LFSs and excitations because, when an excitation occurs inside a LFS, its movement may distort the LFS, potentially causing it to no longer be detected. If the LFS is no longer detected, its separation from the excitation cannot be measured, which would severely impact our analysis. The method we have implemented avoids this issue.

From this labeling, we calculate the conditional probability that a particle is in an excitation given that it belongs to a LFS, $P(EX|LFS)$, as well as the probability of finding excitations $P(EX)$. Probabilities are computed for each configuration along the trajectory. The ratio $P(EX|LFS)/P(EX)$ indicates the probability that excitations overlap with LFS. For each temperature, we compute the average of that ratio over the ten independent trajectories, each comprising 1000 configurations.

We also compute the distance $d$ between an excitation and its closest LFS center, defined as the particle closest to the geometric center of the LFS. In the insets of Fig. 1(b), the LFS centers are shown in pink, and the geometric center with a black dot. For the antiprism, the central particle of the LFS coincides with the geometric center. For the defective icosahedron, the central particle of the LFS is $0.45\sigma$ away from the geometric center.

## III. RESULTS

We begin our results section by discussing the glass-forming behavior of the systems under consideration. Specifically, we report an increase in relaxation time and LFS population, as well as a decrease in excitation concentration, with cooling or compression. Next, we examine the spatial relationship between LFS and excitations, starting with visual observations. We then discuss the growing spatial separation between excitations and LFS. Finally, we investigate the local packing of particles within excitations and LFS to rationalize this separation.

### A. The proportion of LFS and excitations at deep supercooling

In Fig. 1(a) we show the logarithm of the relaxation time $\tau_\alpha$ with respect to the scaled inverse temperature $T_{vft}/T$ for the KA mixtures and scaled reduced pressure $Z/Z_{vft}$ for the experimental hard-sphere colloidal system. The scaled temperature and reduced pressure are obtained by fitting the relaxation time data by a Vogel-Fulcher-Tamman (VFT) form

$$\tau_\alpha^{sim} = \tau_0 \exp\left(\frac{DT_{vft}}{T - T_{vft}}\right), \quad \tau_\alpha^{exp} = \tau_0 \exp\left(\frac{DZ}{Z_{vft} - Z}\right) \quad (5)$$

for simulations and experiments, respectively, with $D$ a system-dependent constant. We focus on the regime below the mode-coupling crossover, highlighted with a blue shading. The mode-coupling crossover temperature is taken from Ortlieb *et al.* [20]: $T_{mct} = 0.55 \pm 0.09$ and $0.7 \pm 0.1$ for the KA 2:1 and 3:1 mixtures, respectively. For experiments, we have $\phi_{mct} = 0.58$ [50] which corresponds to a reduced pressure $Z_{mct} = 23.23$.

Next, we turn to the evolution of the LFS population, defined as the number of long-lived LFS $N_{LFS}$ divided by the number of particles $N$. In Fig. 1(b) we see that the population of LFS grows with supercooling in all systems. At the lowest temperature, one particle in three belongs to a long-lived LFS.

Regarding excitations, DF theory predicts that their concentration $c_a$ decreases exponentially with the inverse temperature or reduced pressure [22]. This scaling was shown to hold below the MCT crossover temperature [20]. We report in Fig. 1(c) the data obtained from identifying excitations in inherent state (IS) trajectories in simulations. We confirm that our data is consistent with the DF scaling.

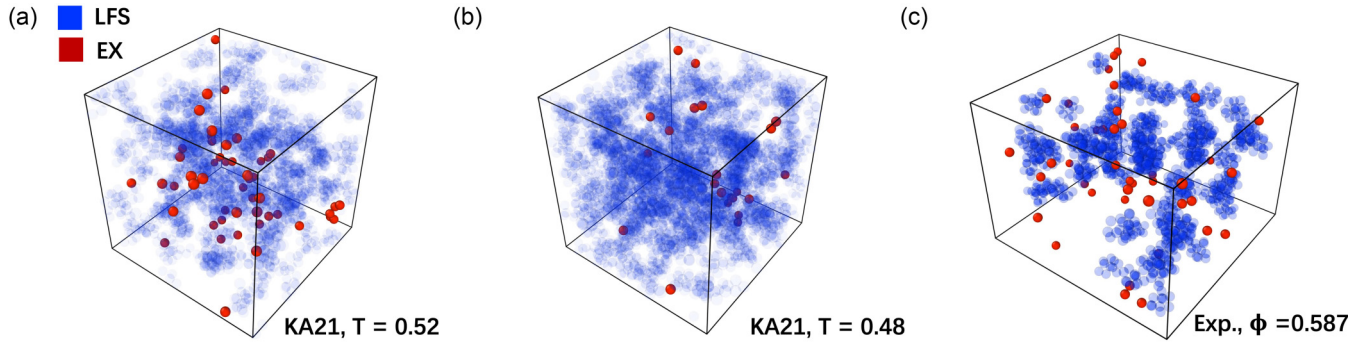


FIG. 2. Representative snapshots showing in blue the particles that belong to a long-lived LFS, and all the excitation particles found in the trajectory in red. Simulations at (a) $T = 0.52$ and (b) $T = 0.48$ in the KA 2:1 mixture and (c) in an experimental colloidal system at $\phi = 0.587$.

### B. The anticorrelation between LFS and excitations

To better understand the relationship between excitations and LFS, we first discuss the snapshots taken from simulations and the experiment which are shown in Fig. 2. From (a) to (b), we observe that as the temperature is lowered, the LFS population increases while the excitation concentration decreases, illustrating the findings in Figs. 1(b) and 1(c). Furthermore, excitations and LFS are spatially separated. This suggests that the excitations and LFS do not overlap.

To quantify these observations, we report in Fig. 3 the temperature/pressure dependence of the conditional probability $P(EX|LFS)$, which measures the likelihood that a long-lived LFS particle participates in an excitation. To compare across different levels of supercooling, the data is normalized by the overall probability of finding excitations, $P(EX)$. This conditional probability is found to be very small, with $P(EX|LFS)/P(EX) \in [0, 0.0401]$ in simulations, as shown with full lines in Fig. 3.

An anticorrelation between LFS and excitations was reported by Ref. [20]. We show their KA 2:1 data in Fig. 3 (dashed line). By considering long-lived LFS and IS trajectories to detect LFS and excitations, we find a much stronger anticorrelation than anticipated. Instead, the dashed line in Fig. 3 corresponds to all LFS and excitations found in thermal trajectories. We examined the respective contributions of IS trajectories and long-lived LFS to the correlation. While analyzing IS trajectories and all LFS affects the results (with the normalized conditional probability decreasing to 0.45−0.35 as supercooling increases), the primary difference arises from focusing on long-lived LFS, particularly at low temperatures. Our finding that long-lived and IS LFS strongly anticorrelate with excitations mediating dynamic relaxation may relate to the work of Alkemade *et al.* [36]. In their study, the authors observed an improved dynamic predictability when considering IS or "cage-state" configurations, the latter reflecting aspects of long livedness.

Such an anticorrelation is also found in the experimental data, see the blue points in Fig. 3. For the experiments, we can only consider thermalized trajectories and long-lived LFS, hence the higher values reported.

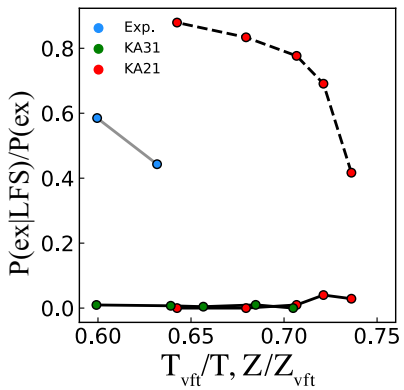


FIG. 3. Anticorrelation between LFS and excitations. Thermalized/instantaneous data from Ortlieb *et al.* [20] (black dashed line with red data points). Experimental data with long-lived LFS is shown with the blue data points. Solid lines correspond to the anticorrelation between long-lived LFS and excitations in the inherent states.

### C. The spatial separation between LFS and excitations

To further probe the anticorrelation between LFS and excitations and their spatial separation, we compute the distance between excitations and their closest LFS center. Figures 4 and 6(a) render some typical scenarios where the excitation takes place inside or outside a LFS, for simulations and experiments, respectively.

We compute the probability distribution $P_{ex}(d)$, shown in Fig. 5(a). While the raw data suggests that the distance between excitations and LFS decreases with supercooling, note that this is expected of any particle, given that the LFS

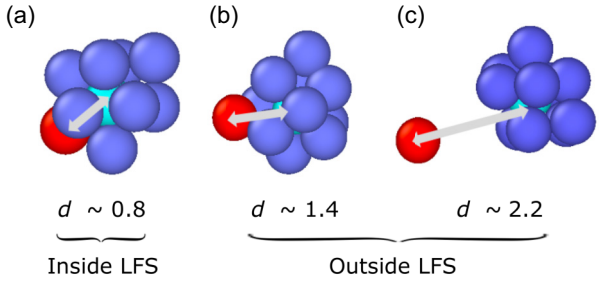


FIG. 4. Renderings of some typical examples of excitations inside LFS (a) and outside LFS (b), (c), with $d$ the distance from an excitation particle (red) and its closest LFS center (cyan).

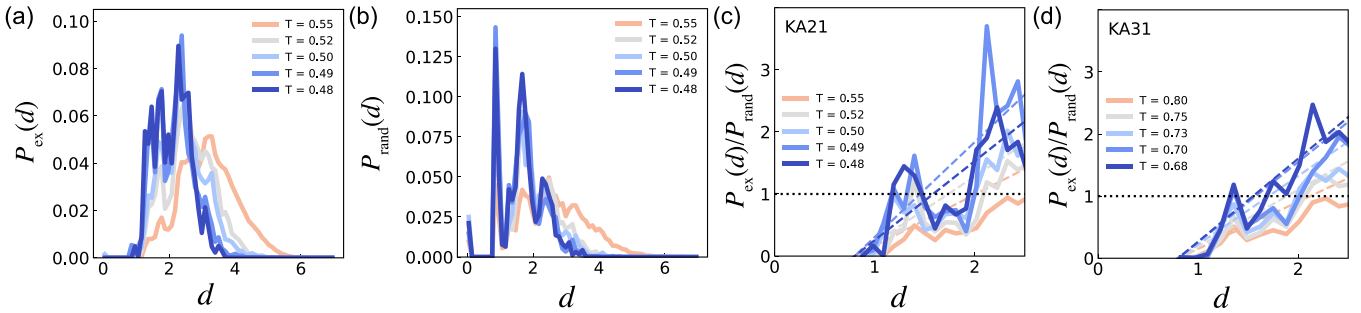


FIG. 5. The spatial relationship between excitations and LFS in simulations. We report the probability distribution of the distance $d$ between a given particle and its closest LFS center. We consider particles that are: (a) excitations, and (b) randomly chosen. (c) The normalized distribution of excitation–LFS center distance, i.e., the ratio of (a) over (b). (d) same as (c) for the KA 3:1 mixture. Dashed lines are linear fits. The horizontal line separates distances from a LFS where excitations are enhanced (above) or suppressed (below).

proportion increases with cooling. To compensate for this, we normalize the data by $P_{\text{rand}}(d)$, the probability distribution of the distance between a random particle and its closest LFS center, shown in Fig. 5(b). It is related to the pair distribution function, but constrained to one particle being a LFS center. It thus exhibits peaks at multiples of the particle diameters.

The resulting data for $P_{\text{ex}}(d)/P_{\text{rand}}(d)$, shown in Fig. 5(c), illustrates how the probability of finding an excitation varies with distance $d$. The horizontal dotted line separates distances at which the probability of finding an excitation is enhanced or suppressed. We find that as the temperature decreases, excitations occur increasingly far from the LFS. The probability of having an excitation inside a LFS, corresponding to $d < 1$ and illustrated in Fig. 4(a), is zero. We identify two peaks of enhanced probability, located around $d \sim 1.4$ and $d \sim 2.2$, with the second peak higher and increasing with supercooling. This demonstrates a larger probability of finding excitations further away from LFS. The locations of these peaks corresponding to excitation-LFS distances is shown in Figs. 4(b) and 4(c), respectively.

To highlight the increasing spatial separation between excitations and LFS, we fit the ratio of probabilities by a linear function, shown with dashed lines. We find that there is a trend that excitations are more likely to occur outside LFS, and even more so at low temperatures. This spatial separation between LFS and excitations is also observed in the KA 3:1 mixture, see Fig. 5(d), and the experimental colloidal system as shown in Fig. 6. We further performed simulations of the common KA 4:1 mixture, and find a similar behavior, in the form of a spatial separation between LFS and excitations, see Fig. 9 in the Appendix. However, there is rather little variation with temperature: due to the effects of crystallization in the 4:1 composition [39], the lowest temperature that we consider is $T = 0.4$. Here the structural relaxation time compared to that at the mode-coupling crossover is $\tau_\alpha(T = 0.4)/\tau_\alpha(T_{\text{mct}}) \sim 30$. However in the case of the 2:1 composition, we reach $\tau_\alpha(T = 0.48)/\tau_\alpha(T_{\text{mct}}) \sim 800$. We attribute the smaller change in the 4:1 mixture to this weaker degree of supercooling.

Thus, for all systems considered here, there is a tendency for excitations to occur increasingly further away from LFS upon supercooling. This is the main result of our study.

### D. Voronoi cell volumes

To investigate why excitations are more likely to occur outside LFS, we compute the volume of the Voronoi cell for each particle. In Fig. 7, we separate A (a) and B (b) particles of the KA 2:1 composition, and report for each the distribution of Voronoi volumes of excitation of LFS particles. Although the distributions overlap, there is a clear trend of LFS particles having smaller Voronoi volumes, indicating better packing. In contrast, excitations show larger Voronoi volumes, suggesting poorer packing. This trend is particularly pronounced for the smaller B particles. We show the case for the KA 3:1 composition in Fig. 10 of the Appendix. For the experimental data, errors in coordinate tracking complicate this analysis. Moreover, for a given coordinate, we do not know the diameter of the specific particle in this polydisperse system [10,11].

## IV. DISCUSSION

We have investigated the spatial relationship between locally favored structures and excitations in simulations and experiments on model glassformers. This work was motivated by the recent observation of a significant anticorrelation between excitations and LFS [20]. This seems to be stronger

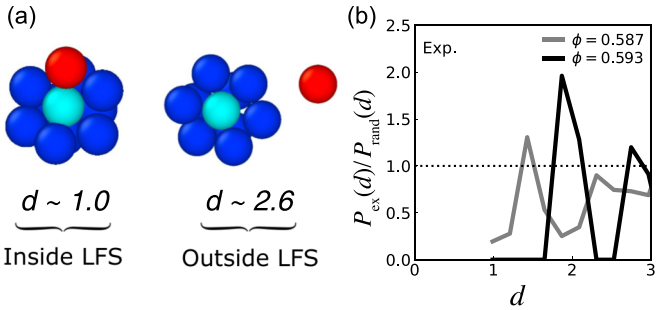


FIG. 6. The spatial relationship between excitations and LFS for the experiments. (a) Some typical scenarios of particles inside LFS and outside LFS, with $d$ the distance from one particle and its closest LFS center. (b) Scaled excitation-LFS center distance. This corresponds to Figs. 5(c) and 5(d).

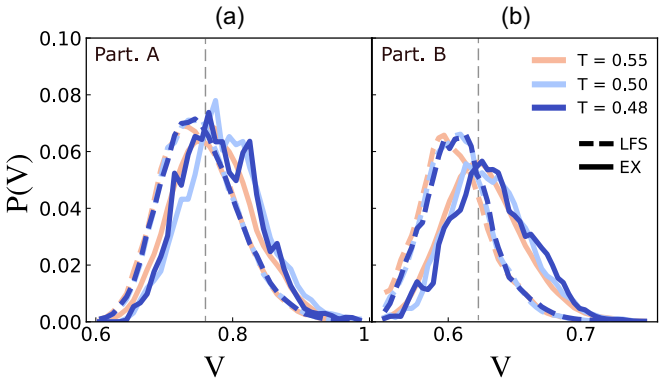


FIG. 7. Volumes of Voronoi cells for particles in LFS (dashed lines) and excitations (solid lines) in the KA 2:1 composition. The probability distribution of (a) A and (b) B particles. The vertical black line is the average over all (A or B) particles. Data for the KA 3:1 mixture is provided in Fig. 10.

than is the case for earlier work which examined the relation between local structure and dynamic heterogeneity at weaker supercooling [46,51].

Here we found a significant anticorrelation between long-lived LFS and excitations. This is stronger than that observed previously [20], due to our use of long-lived LFS and using inherent state coordinates. Some comments are in order here. In a series of papers, Speck and coworkers explored the dynamical phase transition of dynamic facilitation theory in a number of model glassformers in both simulations and the experiment [26,29,37,52–54]. This transition—obtained using short (a few $\tau_\alpha$) and small (typically around 100–200 particles) trajectories—exists between a so-called active phase (similar to the normal supercooled liquid) and an inactive phase, whose dynamics are too slow to be measured on the simulation timescale. In the work of Speck and collaborators, this transition is driven by the time-averaged population of LFS, (or by dynamics, as obtained previously [55,56]). Therefore, the anticorrelation between excitations (a feature of the active phase) and long-lived LFS (which are likely related to the time-averaged LFS of the inactive phase) may be taken as consistent with the dynamical phase transition. We therefore expect that long-lived LFS are some measure of local stability in the supercooled liquid.

The deeper supercooling now possible in both experiment and computer simulation enables us to identify excitations (which are hard to detect for $T > T_{\rm mct}$ and $Z < Z_{\rm mct}$). Earlier work often struggled to find a significant coupling between local structure and dynamic heterogeneity [46,51].

It has been found that there is a rather weaker anticorrelation between LFS and cooperatively rearranging regions (CRRs) which are the elementary units of relaxation in RFOT and Adam-Gibbs thermodynamic-based theories [20]. If we imagine that the long-lived LFS are representative of the emerging solid glass, the enhanced anticorrelation of the excitations with respect to the CRRs raises questions about these relaxation mechanisms. It has been suggested that CRRs may be comprised of many excitations [20]. It should be noted that the trajectories we can analyze here are much shorter than the structural relaxation time $\tau_\alpha$ and indeed the timescale associated with CRRs, which reaches $1.1 \times 10^5$ LJ time units for the lowest temperature studied [20]. By construction, the LFS lifetimes we measure are shorter than the trajectories. While we believe that we have a reasonable criterion to exclude short-lived LFS, it would certainly be desirable to be able to apply our analysis on longer timescales up to the structural relaxation time. Such timescales of course present great challenges for the frequency of sampling that we use here. Here, we have focused on the excitations, but the link between excitations and the much longer timescale CRRs, and the LFS remains an intriguing and challenging topic for a future investigation.

## V. CONCLUSION

In this work, we have analysed particle-resolved data from both GPU simulations and experiments in deeply supercooled liquids, with a focus on detecting excitations and identifying long-lived locally favored structures. We have shown that with the decrease in temperature (in simulations) or increase in reduced osmotic pressure (in experiments), the proportion of LFS grows while the proportion of excitations decreases. Moreover, a strong and robust anticorrelation between long-lived LFS and excitations has been identified. By considering inherent states in our computer simulations, we have obtained a stronger anticorrelation than that previously found [20]. To further probe this anticorrelation, we have computed the distance between excitations and long-lived LFS and excitations. Notably, excitations are more likely to occur outside long-lived LFS, demonstrating there is a spatial separation between the two. This spatial separation may be attributed to the well-packed nature of long-lived LFS, as revealed by the analysis of the volumes of the Voronoi cells for each particle.

Our work provides a picture of structural relaxation via excitations occurring in regions of the system outside long-lived LFS. We hope this will stimulate further investigations of the relationship between structure and dynamics in the deeply supercooled regime of glass-forming systems which is now accessible.

## ACKNOWLEDGMENTS

The authors would like to acknowledge Ludovic Berthier, Thomas Speck, and Gilles Tarjus for insightful discussions. D.L. gratefully acknowledges Université de Recherche Paris Sciences et Lettres for financial support. C.P.R. would like to acknowledge the Agence Nationale de la Recherche for the provision of the grant DiViNew.

## DATA AVAILABILITY

The data that support the findings of this article are not publicly available upon publication because it is not technically feasible and/or the cost of preparing, depositing, and hosting the data would be prohibitive within the terms of this research project. The data are available from the authors upon reasonable request.

## APPENDIX

This Appendix presents details of characteristics of the systems considered. Tables I and II provide the Vogel-Fulcher-Tamman (VFT) parameters and the scaling of the fraction of particles in excitations, respectively. Figure 8 shows the cumulative probability distribution of LFS lifetime in various systems. Figures 9 and 10 show the spatial separation between LFS and excitations and Voronoi cell volumes for systems not shown in the main text, respectively.

TABLE I. VFT parameters fitted to the various systems considered.

| | KA 2:1 | KA 3:1 | Experiment |
|---|---|---|---|
| $T_{\mathrm{VFT}}$ or $Z_{\mathrm{VFT}}$ | 0.35 | 0.48 | 41 |
| $\tau_0$ | 0.09 | 0.07 | 0.63 |
| $D$ | 6.17 | 6.88 | 5.09 |

TABLE II. Scaling of the fraction of particles in excitations.

| | KA 2:1 | KA 3:1 | Experiment |
|---|---|---|---|
| $T_{\mathrm{on}}$ or $Z_{\mathrm{on}}$ | 0.75 | 1.2 | 23 |
| $E_a$ | 5.96 | 8.30 | 1.19 |

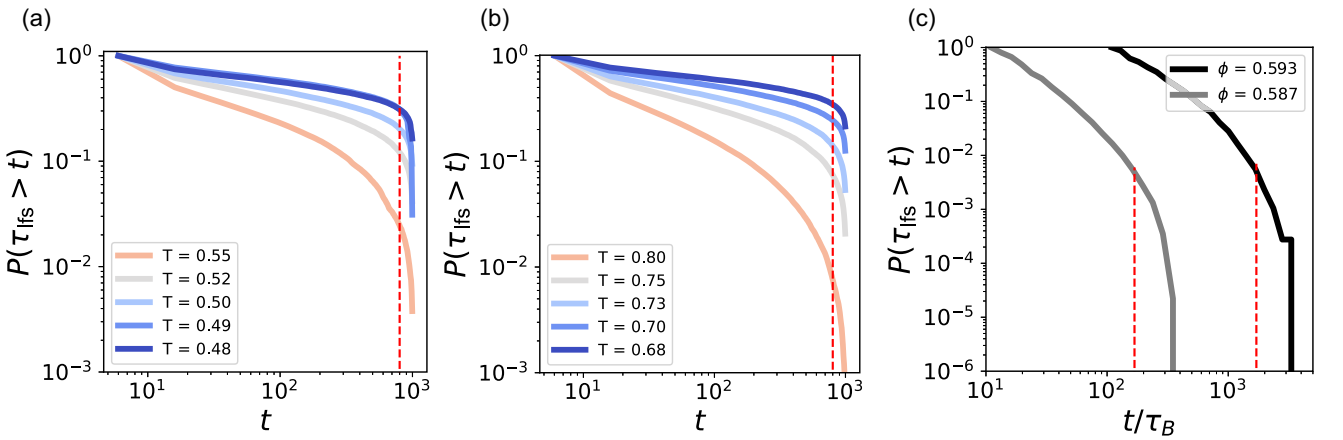


FIG. 8. The cumulative probability distribution of LFS lifetime $\tau_{\mathrm{lfs}}$ in simulations of the KA system at (a) 2:1, (b) 3:1, and (c) colloidal experiments. The timescale corresponds to $P(\tau_{\mathrm{lfs}} > t) = 1$ differs due to the different time separation between frames. LFS with a lifetime greater than the vertical dashed red lines are defined as long-lived.

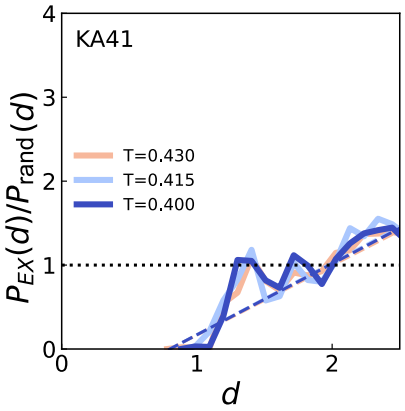


FIG. 9. The normalized probability distribution of the distance $d$ from the LFS center in the KA 4:1 system.

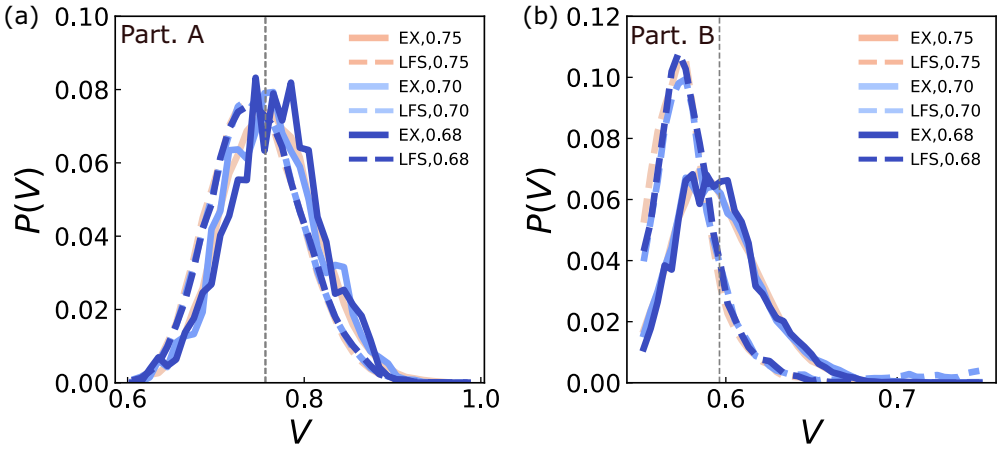


FIG. 10. Volumes of Voronoi cells for particles in LFS and excitations in the KA 3:1 composition. (a) The probability distribution of A particles. (b) The probability distribution of B particles. The vertical black line is the average of all particles. Solid lines are particles in excitations, dashes are particles in LFS.


[1] L. Berthier and G. Biroli, Rev. Mod. Phys. **83**, 587 (2011).
[2] G. Adam and J. Gibbs, J. Chem. Phys. **43**, 139 (1965).
[3] V. Lubchenko and P. G. Wolynes, Annu. Rev. Phys. Chem. **58**, 235 (2007).
[4] D. Chandler and J. P. Garrahan, Annu. Rev. Phys. Chem. **61**, 191 (2010).
[5] T. Speck, J. Stat. Mech. (2019) 084015.
[6] G. Tarjus, S. A. Kivelson, Z. Nussinov, and P. Viot, J. Phys.: Condens. Matter **17**, R1143 (2005).
[7] C. P. Royall and S. R. Williams, Phys. Rep. **560**, 1 (2015).
[8] M. Leocmach and H. Tanaka, Nat. Commun. **3**, 974 (2012).
[9] G. L. Hunter and E. R. Weeks, Rep Prog Phys 31 (2012).
[10] A. Ivlev, H. Lowen, G. E. Morfill, and C. P. Royall, *Complex Plasmas and Colloidal Dispersions: Particle-Resolved Studies of Classical Liquids and Solids* (World Scientific Publishing Co., Singapore, 2012).
[11] C. P. Royall, P. Charbonneau, M. Dijkstra, J. Russo, F. Smallenburg, T. Speck, and C. Valeriani, Rev. Mod. Phys. **96**, 045003 (2024).
[12] S. Gokhale, A. K. Sood, and R. Ganapathy, Adv. Phys. **65**, 363 (2016).
[13] D. R. Reichman and P. Charbonneau, J. Stat. Mech. (2005) P05013.
[14] A. Ninarello, L. Berthier, and D. Coslovich, Phys. Rev. X **7**, 021039 (2017).
[15] B. Guiselin, C. Scalliet, and L. Berthier, Nat. Phys. **18**, 468 (2022).
[16] C. Scalliet, B. Guiselin, and L. Berthier, Phys. Rev. X **12**, 041028 (2022).
[17] N. P. Bailey, T. S. Ingebrigtsen, J. S. Hansen, A. A. Veldhorst, L. Bøhling, C. A. Lemarchand, A. E. Olsen, A. K. Bacher, L. Costigliola, U. R. Pedersen, H. Larsen, J. C. Dyre, and T. B. Schrøder, SciPost Phys. **3**, 038 (2017).
[18] G. Brambilla, D. El Masri, M. Pierno, L. Berthier, L. Cipelletti, G. Petekidis, and A. B. Schofield, Phys. Rev. Lett. **102**, 085703 (2009).
[19] J. E. Hallett, F. Turci, and C. P. Royall, Nat. Commun. **9**, 3272 (2018).
[20] L. Ortlieb, T. S. Ingebrigtsen, J. E. Hallett, F. Turci, and C. P. Royall, Nat. Commun. **14**, 2621 (2023).
[21] M. R. Hasyim and K. K. Mandadapu, Proc. Natl. Acad. Sci. **121**, e2322592121 (2024).
[22] A. S. Keys, L. O. Hedges, J. P. Garrahan, S. C. Glotzer, and D. Chandler, Phys. Rev. X **1**, 021013 (2011).
[23] M. R. Hasyim and K. K. Mandadapu, J. Chem. Phys. **155**, 044504 (2021).
[24] S. Gokhale, K. Hima Nagamanasa, R. Ganapathy, and A. Sood, Nat. Commun. **5**, 4685 (2014).
[25] K. Hima Nagamanasa, S. Gokhale, A. Sood, and R. Ganapathy, Nat. Phys. **11**, 403 (2015).
[26] F. Turci, C. P. Royall, and T. Speck, Phys. Rev. X **7**, 031028 (2017).
[27] L. Berthier, P. Charbonneau, D. Coslovich, A. Ninarello, M. Ozawa, and S. Yaida, Proc. Natl. Acad. Sci. USA **114**, 11356 (2017).
[28] L. Berthier, M. Ozawa, and C. Scalliet, J. Chem. Phys. **150**, 160902 (2019).
[29] C. P. Royall, F. Turci, and T. Speck, J. Chem. Phys. **153**, 090901 (2020).
[30] J.-P. Bouchaud, arXiv:2402.01883.
[31] A. Widmer-Cooper and P. Harrowell, Phys. Rev. Lett. **96**, 185701 (2006).
[32] L. Berthier and R. L. Jack, Phys. Rev. E **76**, 041509 (2007).
[33] R. L. Jack, A. J. Dunleavy, and C. P. Royall, Phys. Rev. Lett. **113**, 095703 (2014).
[34] A. J. Dunleavy, K. Wiesner, R. Yamamoto, and C. P. Royall, Nat. Commun. **6**, 6089 (2015).
[35] G. M. Hocky, D. Coslovich, A. Ikeda, and D. R. Reichman, Phys. Rev. Lett. **113**, 157801 (2014).
[36] R. M. Alkemade, F. Smallenburg, and L. Filion, J. Chem. Phys. **158**, 134512 (2023).
[37] T. Speck, A. Malins, and C. P. Royall, Phys. Rev. Lett. **109**, 195703 (2012).

[38] J. E. Hallett, F. Turci, and C. P. Royall, J. Stat. Mech. (2020) 014001.
[39] T. S. Ingebrigtsen, J. C. Dyre, T. B. Schrøder, and C. P. Royall, Phys. Rev. X **9**, 031016 (2019).
[40] S. Plimpton, J. Comput. Phys. **117**, 1 (1995).
[41] A. P. Thompson, H. M. Aktulga, R. Berger, D. S. Bolintineanu, W. M. Brown, P. S. Crozier, P. J. in 't Veld, A. Kohlmeyer, S. G. Moore, T. D. Nguyen, R. Shan, M. J. Stevens, J. Tranchida, C. Trott, and S. J. Plimpton, Comput. Phys. Commun. **271**, 108171 (2022).
[42] C. P. Royall, S. R. Williams, and H. Tanaka, J. Chem. Phys. **148**, 044501 (2018).
[43] L. Berthier and T. A. Witten, Phys. Rev. E **80**, 021502 (2009).
[44] A. Malins, S. R. Williams, J. Eggers, and C. P. Royall, J. Chem. Phys. **139**, 234506 (2013).
[45] D. Coslovich and G. Pastore, J. Chem. Phys. **127**, 124504 (2007).
[46] A. Malins, J. Eggers, H. Tanaka, and C. P. Royall, Faraday Discuss. **167**, 405 (2013).
[47] P. Crowther, F. Turci, and C. P. Royall, J. Chem. Phys. **143**, 044503 (2015).
[48] C. P. Royall, A. Malins, A. J. Dunleavy, and R. Pinney, J. Non-Cryst. Solids **407**, 34 (2015).
[49] A. Malins, Ph.D. thesis, University of Bristol, 2013.
[50] W. van Megen, T. C. Mortensen, S. R. Williams, and J. Müller, Phys. Rev. E **58**, 6073 (1998).
[51] B. Charbonneau, P. Charbonneau, and G. Tarjus, Phys. Rev. Lett. **108**, 035701 (2012).
[52] R. Pinchaipat, M. Campo, F. Turci, J. E. Hallett, T. Speck, and C. P. Royall, Phys. Rev. Lett. **119**, 028004 (2017).
[53] F. Turci, T. Speck, and C. P. Royall, Eur. Phys. J. E **41**, 54 (2018).
[54] M. Campo and T. Speck, J. Chem. Phys. **152**, 014501 (2020).
[55] L. O. Hedges, R. L. Jack, J. P. Garrahan, and D. Chandler, Science **323**, 1309 (2009).
[56] T. Speck and D. Chandler, J. Chem. Phys. **136**, 184509 (2012).